Solar Energy 206 (2020) 732–740

Contents lists available at ScienceDirect

Solar Energy

journal homepage: www.elsevier.com/locate/solener

From room to roof: How feasible is direct coupling of solar-battery power unit under variable irradiance?

Oleksandr Astakhov*, Tsvetelina Merdzhanova, Li-Chung Kin, Uwe Rau

Institut für Energie- und Klimaforschung 5 – Photovoltaik (IEK-5), Forschungszentrum Jülich GmbH, 52425 Jülich, Germany

ARTICLE INFO

Keywords:
Solar battery
Direct coupling
Power matching
Variable irradiance

ABSTRACT

Integration of photovoltaics (PV) with electrical energy storage (battery) is a straightforward approach to turn intermittent power source into stable power supply. Power coupling, or power matching, between PV-device, a battery, and a load is most frequently performed with aid of maximum power point tracking (MPPT) electronics. MPPT electronics provides high flexibility as for PV and load impedances, and irradiance, however, it brings in additional cost, and complexity, power overhead, potential reliability issues, and interference signals. On the other hand, direct coupling via preselection of PV and battery parameters is a simple scalable and highly efficient alternative to MPPT for a specific set of conditions. We explore with modeling how far a directly coupled PV-battery unit can stay power-matched under various conditions, and demonstrate feasibility of excellent power matching over orders of magnitude of irradiance and a wide range of load resistances. Both a PV-harvester in an office room with low irradiance, non-demanding load, and high autonomy, and a PV-system on a roof with high irradiance, demanding load, and partial autonomy, can operate efficiently without MPPT electronics if an appropriate battery is included. This result emphasizes the role of a battery as an impedance matching element besides storage functionality in a directly matched PV-system.

1. Introduction

Integration of photovoltaics (PV) with electrochemical energy storage (battery) is a straightforward approach to turn intermittent power sources into a stable power supply. PV-battery integration at different levels and scales is widely discussed in literature (Dennler et al., 2007; Guo et al., 2012; Gurung et al., 2017; Gurung and Qiao, 2018; Hauch et al., 2002; Hu et al., 2019; Kin et al., 2019; Li et al., 2016a; Li et al., 2018; Li et al., 2016b; Liu et al., 2012; Vega-Garita et al., 2019; Zeng et al., 2020). Ranging from indoor applications for modern concepts of "smart houses" or internet of things (IoT) (Agbo et al., 2016a, 2016b; Alippi et al., 2011; Belu, 2012; Bogue, 2012; Chung et al., 2019; Kin et al., 2019; Sandbaumhuter et al., 2017) up to typical field applications (Li et al., 2019; Merei et al., 2016; Millet et al., 2019; Weniger et al., 2014) a PV-battery unit has to ensure proper power coupling of a PV device to a battery and finally a load. Proper power coupling, or power matching, is achieved when input impedance of a load equals to the characteristic resistance of a PV module and maximum possible power is delivered to the load. The problem of power coupling has been extensively addressed in literature for decades. Main solutions include most common matching with aid of maximum power point tracking (MPPT) electronics (El Fadil and Giri, 2011; Gurung et al., 2017; Hua et al., 2003; Kin et al., 2019; Masoum et al., 2002; Shao et al., 2009), "direct coupling" / "direct impedance matching" (Agbo et al., 2016a, 2016b; Appelbaum, 1989; Applebaum, 1987; Azzolini and Tao, 2018; Clarke et al., 2009; Dennler et al., 2007; Gibson and Kelly, 2008; Hauch et al., 2002; Hu et al., 2019; Jaboori et al., 1991; Kakimoto and Asano, 2017; Khouzam et al., 1991; Khouzam, 1990; Khouzam and Khouzam, 1991; Kou et al., 1998; Li et al., 2018; Liu et al., 2012; Maeda et al., 2012; Maroufmashat et al., 2014; Mokeddem et al., 2011; Sandbaumhuter et al., 2017; Su et al., 2016; Tiwari and Kalamkar, 2016; Wang et al., 2016), and in some cases their combinations (Dehbonei et al., 2009). Even though the MPPT solution provides high flexibility for photovoltaics in terms of load impedance, irradiance, and temperatures, it comes with additional cost and complexity of the system, power overhead (power consumed by MPPT), potential reliability issues and interference signals in the power network. The power overhead related to MPPT units may be a critical issue for small scale PV-battery device even with high quality equipment (Kin et al., 2019).

Direct coupling of a PV-battery requires preselection of parameters of a PV module/array and a load and is reported for coupling of PV devices to batteries (Agbo et al., 2016a, 2016b; Azzolini and Tao, 2018;

* Corresponding author.
E-mail addresses: o.astakhov@fz-juelich.de (O. Astakhov), t.merdzhanova@fz-juelich.de (T. Merdzhanova), l.kin@fz-juelich.de (L.-C. Kin), u.rau@fz-juelich.de (U. Rau).

https://doi.org/10.1016/j.solener.2020.06.033
Received 19 February 2020; Received in revised form 4 June 2020; Accepted 7 June 2020

Dennler et al., 2007; Hauch et al., 2002; Hu et al., 2019; Kakimoto and Asano, 2017; Khouzam and Khouzam, 1991; Li et al., 2018; Liu et al., 2012; Paul Ayeng'o et al., 2019; Sandbaumhuter et al., 2017) and electrolyzers (Clarke et al., 2009; Gibson and Kelly, 2008; Maeda et al., 2012; Maroufmashat et al., 2014; Smirnov et al., 2016; Su et al., 2016; Urbain et al., 2016; Urbain et al., 2014). It has been suggested in several works that MPPT is not required for variety of systems and conditions (Agbo et al., 2016a, 2016b; Averbukh et al., 2012; Khouzam et al., 1991; Khouzam, 1990; Paul Ayeng'o et al., 2019). Direct coupling reduces system complexity and cost, may provide high reliability and highest energy efficiency. The system is free of interference signals or power fluctuations related to MPPT operation. These advantages come at a cost of system flexibility, in terms of the load parameters and limited range of PV module/array operating conditions. The limits of the operating conditions however are not well explored in the literature. In our work we study numerically how performance of a directly coupled PV-battery system depends on irradiance and power demand of the load varied over wide range. We explore how far a PV-battery combination can stay power-matched under variable irradiance and load, and study feasibility of the direct coupling as a practical solution. In order to address these issues, we considered two distinct cases of PV-battery applications. The first case is a "PV-harvester" in a room – a relatively small-scale PV module integrated with a battery to provide autonomous function of a "smart device" with low power demand predominantly indoors, e.g. in an office room and analyzed in the "Room" section of the paper. The second case is an outdoors "PV-system" – a PV module combined with a battery to power highly demanding load under high irradiance, with optional energy autonomy – traits typical for a residential PV-system on a roof analyzed in the "Roof" section of the paper. These two cases are distinguished from the point of view of relative load power demand while system scale is taken out of consideration with normalization of the analysis by PV module area. In both cases we consider a basic unit of a PV module with minimal number of cells coupled to a single secondary battery cell. These units can be part of a larger panel or system or used individually. Calculations are performed for battery open circuit voltage range of 3.1–4.6 V relevant for modern commercial Li-ion cells.

The paper consists of three parts. First, basic design, energy balance and scaling of equivalent load resistance for the PV-battery power unit is presented. Next, models, simulation procedure, and coupling quantification are described. Finally, simulation results for both the "PV-harvester" and "PV-system" are discussed.

2. Energy balance and design of a PV-battery power supply

2.1. PV power output as a function of irradiance.

Power output and efficiency of a solar cell depends on irradiance, spectrum (Agbo et al., 2017; Bahrami-Yekta and Tiedje, 2018; Bunea et al., 2006; Merten et al., 1998) and temperature (Dupré et al., 2017). For the sake of simplicity spectral and thermal variations are left out of consideration, even though significant efficiency improvements are observed under modern indoor lighting (Agbo et al., 2017). To illustrate the range of available power densities, the maximum power density P_{max} for a solar cell with industrially available efficiency $\eta = 21\%$ is calculated for approx. four orders of magnitude of total irradiance E_e in fractions of 1 sun (International, 2012) and illuminance E_V in lux, and presented in Fig. 1. Details of the simulations are presented in the section 3. Colored areas in Fig. 1 represent various typical illuminance conditions (Awasthi, 2014; Standartization, E.c.f, 2002, 2014). The cell shows nearly linear dependence of P_{max} on irradiance in the range from 1 sun down to 0.01 sun and sublinear reduction at lower E_e due to the effect of shunt resistance (Bunea et al., 2006). At the bottom of Fig. 1 projected irradiance ranges for PV-harvester and PV-system are presented with blue arrows. Projected irradiance on a PV-harvester ranges from 0.003 sun ($E_V = 300$ lx – typical requirement for an office room

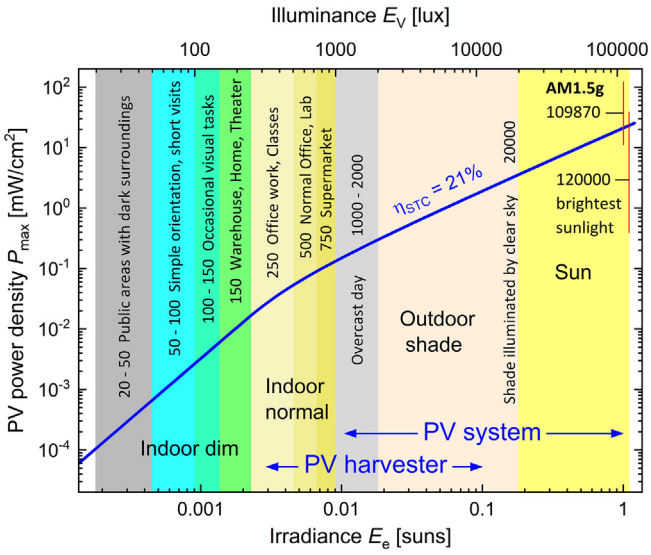

Fig. 1. Maximum output power density of a solar cell with standard test conditions (STC) (International, 2012) efficiency $\eta = 21\%$ as a function of irradiance E_e and illuminance E_V. Areas of different colors approximately represent denoted illuminance conditions (Awasthi, 2014; Standartization, E.c.f, 2002, 2014)). Numbers in the graph are E_V values in lux. Blue arrows at the bottom represent approximately target operation ranges for PV-harvester and PV-system. (For interpretation of the references to colour in this figure legend, the reader is referred to the web version of this article.)

(Awasthi, 2014; Standartization, E.c.f, 2002, 2014) till approx. 0.1 sun for indoor irradiance on a Sunny day. Projected irradiance on a PV-system is taken the range of 0.01–1 sun.

2.2. Design and energy balance of a PV-battery unit

Block diagram of the PV-Battery device under consideration is presented in Fig. 2(a) where red arrows show energy transfer under sufficient irradiance. Power of light P_{Light} is converted into electric power P_{PV} in a PV module and is divided into power consumed in a load P_L and power of battery charge P_{Bc}. Blue arrow indicates discharge of the battery P_{Bd} powering the load when PV module is idle in the dark. Circuit diagram in Fig. 2(b) represents the simplest realization of the PV-battery device, where current from a PV module is divided between a battery and a load. In the simplest case without reverse blocking elements certain battery discharge is expected without illumination through forward biased PV module. However properly designed PV-battery combination has low dark current density (Agbo et al., 2016a, 2016b) which is a matter of optimization and is out of the scope of this paper.

Analysis of power matching in the PV-battery device sketched in Fig. 2 is focused on the generating phase of a 24 h cycle. However, a full 24 cycle has to be considered for meaningful scaling of the PV-battery elements. The energy balance of the system with respect of required degree of autonomy dictates values of effective load resistance R_L and battery capacity C_B per unit area of PV module. Schematic power/energy balance diagram for a projected 24-hour cycle of a PV-battery unit is presented in Fig. 3(a). The 24-hour cycle consists of a light phase $T_l = 8$ h and a dark phase $T_d = 16$ h in our conservative projection for both indoor PV-harvesters and outdoor PV-systems. During T_l a PV module generates power P_{PV} which is divided between a load, consuming P_L, and a battery, charging with P_{Bc}. After the light phase is over the battery discharge P_{Bc} powers the load during the dark phase T_d.

Areas of rectangles in Fig. 3(a) represent total energies of each element for T_l and T_d as follows: E_{PV} is the energy generated by PV module; E_{Ll} is the load energy demand during T_l; E_{Ld} the load energy demand during T_d; E_{Bc} the energy stored in the battery during T_l; E_{Bd}

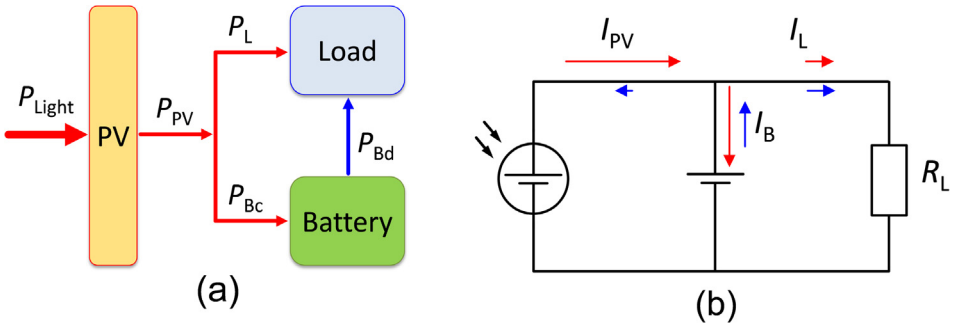

Fig. 2. (a) Block diagram of a PV-battery unit connected to a load. P_{Light} – power of light impinging a PV module; P_{PV}- power generated by the PV module; P_L – power supplied to the load; P_{Bc} – power of battery charge; P_{Bd} – power of battery discharge; (b) Circuit diagram of a directly coupled PV-battery. Red arrows indicate currents under sufficient irradiance, blue arrows – current in dark conditions. I_{PV} – current of PV module; I_L current through the load; I_B – current of the battery; R_L equivalent load resistance. (For interpretation of the references to colour in this figure legend, the reader is referred to the web version of this article.)

the energy delivered by the battery during T_d. The analysis is based on the balance between generated and consumed energy. The battery capacity C_B is assumed to be sufficient to store available E_{Bc} and possible charge–discharge losses are out of consideration. The energy balance throughout a 24-hour cycle is analyzed with a "system energy autonomy factor" f_A – the ratio of energy stored during T_l, E_{Bc}, to the energy demand of the load during T_d, E_{Ld}:

$$f_A = \frac{E_{Bc}}{E_{Ld}} = \frac{E_{PV} - E_{Ll}}{E_{Ld}} = \frac{(P_{PV} - P_L)T_l}{P_L T_d}. \quad (1)$$

f_A takes values in the following characteristic ranges:

- $f_A > 1$ when E_{PV} is higher than total energy demand of a load ($E_{Ll} + E_{Ld}$) and $E_{Bc} > E_{Ld}$ the case of full autonomy with energy redundancy preferable for PV-harvester;
- $1 > f_A > 0$ when E_{PV} is lower than total energy demand of a load ($E_{Ll} + E_{Ld}$) but is still higher than E_{Ll}, which implies $0 > E_{Bc} > E_{Ld}$ the case of partial autonomy usual for grid connected residential PV-systems with storage
- $f_A < 0$ when E_{PV} does not cover energy demand of a load even during light phase T_L, therefore $E_{Bc} < 0$ which has no physical meaning, but indicates that storage is purposeless in the system.

The system autonomy factor f_A calculated as a function of irradiance E_e and projected load power demand P_L presented as a contour plot in Fig. 3(b) is used to determine the feasible range of load power demand for a PV-battery unit. Dashed lines in Fig. 3(b) contour approximately operation conditions of two addressed PV-battery utilization cases: "PV-harvester" providing reliable autonomy in low irradiance for low-power-consumption load, and "PV-system" powering demanding load with optional autonomy predominantly under high irradiance. These two cases are distinguished upon PV-area specific power demand of a load. The system scale is out of consideration. In both cases we consider a basic unit of a PV module with minimal number of cells coupled to a single secondary battery cell. Therefore, operating voltage range is same for both PV-harvester and PV-system and approximately corresponds to the voltage range of contemporary Li-ion cells.

With determined ranges of specific load power demand, the equivalent load resistance R_L can be scaled approximately, taking the common voltage of a commercial Li-ion battery of 3.6 V (Chen et al., 2018; Zhang et al., 2018). According to the PV-area-specific power ranges marked in Fig. 3(b) specific equivalent load resistance R_L of approximately 1 MΩ cm^2 will ensure full autonomy at the lowest irradiance of 0.003 sun in artificially lit office for PV-harvester. For PV-system $R_L \approx 2$ kΩ cm^2 ensures full autonomy at high irradiance and partial autonomy at specific $R_L \approx 1$ kΩ cm^2.

For the case of PV-harvester, high specific R_L allows neglecting the role of load current, and simulate PV-battery coupling as a function of irradiance and battery open circuit voltage. For the PV-system on contrary, R_L is taken into consideration, and PV-battery coupling is analyzed as a function of irradiance and specific load resistance.

Scaling of the battery capacity C_B is carried out considering

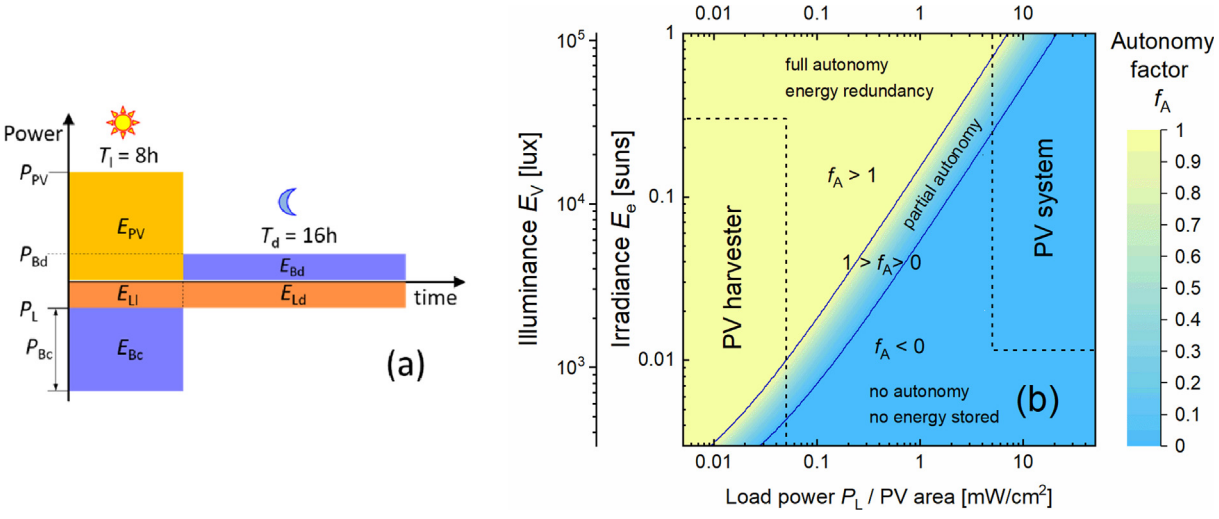

Fig. 3. (a) Schematic illustration of power and energy balance of PV-battery system with load throughout projected 24 h-cycle on time scale. During the light phase T_l power of a PV module P_{PV} is opposed by power demand of a load P_L and power of a battery charge P_{Bc}. During the dark phase T_d, the load power demand P_L is covered by the battery discharge power P_{Bc}. Areas characteristic rectangles represents following energies: E_{PV} – energy generated by PV module; E_{Ll} – load energy demand during T_l; E_{Ld} – load energy demand during T_d; E_{Bc} – energy stored in the battery during T_l; E_{Bd} – energy delivered by the battery during T_d. (b) Energy autonomy factor f_A of PV-battery system as a function of specific load power demand P_L and irradiance E_e calculated for a 21% efficient solar module. See text for details.

autonomy and reliability factors. For critical autonomy $f_A = 1$, $E_{Ll} + E_{Ld} = E_{PV}$, and $P_L(T_l + T_d) = P_{PV}T_l$, C_B is calculated as:

$$C_B = I_L T_d = \frac{P_L T_d}{V_{Bd}} = \frac{P_{PV} T_l T_d}{V_{Bd}(T_l + T_d)}, \quad (2)$$

where V_{Bd} is the battery discharge voltage. For $\eta = 21\%$, $V_{Bd} = 3.5$ V, and $T_l = 8$ h, C_B of 32 mAh per cm^2 of PV provides critical autonomy under 1 sun. At lower irradiance, proportionally lower C_B is required, however battery damage has to be excluded at eventual exposure of a PV-harvester to direct sunlight. Under 1 sun a PV module with $\eta = 21\%$ delivers 5 mA/cm^2 at 4.2 V (typical charging voltage limit of Li-ion battery). Charging rate limit of Li-ion batteries ranges between 1 C and 8 C (Chen et al., 2018). Conservative limit of 1–2 C requires C_B of 2.5–5 mAh per cm^2 of PV. We use compromise $C_B = 20$ mAh for 7 cm^2 PV module, which is within safe charging range at $E_e = 1$ sun and provides full autonomy at $E_e < 0.1$ sun for a PV-harvester.

3. Simulation of power matching in a PV-battery power supply

3.1. Power matching problem

Under proper coupling PV part of the system operates at maximum power point (MPP) and delivers maximum possible power to a battery and/or other load. This requires matching of PV module characteristic resistance to the input impedance of the battery/load combination. Characteristic resistance of the PV module or its MPP varies with irradiance and temperature. Input impedance of the battery/load combination may shift according to the battery state of charge (SOC) or battery current (Li et al., 2016b; Li et al., 2019). Among these factors, irradiance has usually the strongest impact on the system coupling, whereas modern commercial batteries in many cases exhibit flat charge/discharge characteristic, i.e. battery voltage does not change significantly over large range of SOC (Hosono et al., 2007; Julien and Mauger, 2013; Roscher et al., 2011; Sun et al., 2015; Zaghib et al., 2011).

Operating point or working point (WP) for a PV-Battery-load system presented in Fig. 2 can be found with the following equation:

$$I_{PV}(V) = I_B(V) + I_L(V), \quad (3)$$

where I_{PV} is the current of PV module, I_B is the battery current and I_L is the current of the load, V is the voltage equal for all elements in Fig. 2(b).

For PV-harvester with high R_L the equation can be simplified by neglecting I_L:

$$I_{PV}(V) = I_B(V), \quad (4)$$

Solutions of the Equations (3) or (4) give current and voltage of the working point I_{WP} and V_{WP} – the coordinates of a crossing point between the PV module IV and battery IV eventually combined with load IV. This is visually illustrated for the pure PV-battery case in Fig. 4(a), and the PV-battery-load case in Fig. 6(a). Optimal matching is achieved when working point is at the maximum power point of the PV module. In general case WP does not coincide with MPP. The degree, or quality of matching, can be quantified by a "coupling factor" C - the ratio of the working point power P_{WP} to the maximum power P_{MPP} of the PV module:

$$C = \frac{P_{WP}}{P_{MPP}} = \frac{I_{WP} V_{WP}}{I_{MPP} V_{MPP}}. \quad (5)$$

The coupling factor shows how close WP is to MPP, it takes values between 0 and 1 where unity corresponds to perfect matching. The coupling factor is a key parameter used to evaluate power matching in PV-battery combination. In order to find C for PV-battery combination under specific irradiance we simulate IV characteristics of PV module and battery according to the models described below.

3.2. Solar module model

Current-voltage characteristics $I_{PV}(V)$ of a PV module were simulated with one diode model including series and shunt resistances (R_s and R_{sh}) which is described with well-known expression:

$$I_{PV}(V) = I_L - I_0 e^{\frac{q(V + I_{PV} R_s)}{nkT}} - \frac{V + I_{PV} R_s}{R_{sh}}, \quad (6)$$

where I_L is photocurrent, I_0 - dark saturation current, q- elementary charge, V – voltage across the cell, n – diode ideality factor, k – Boltzmann constant and T – absolute temperature. The diode expression (6) is implicit function and is solved numerically.

The solution of (6) is IV-characteristic of a single solar cell and transition to PV module is made with multiplication of the voltage scale by a required number of cells N_C:

$$I_{PVmodule}(V * N_C) = I_{PVcell}(V). \quad (7)$$

Potential increase of series resistance duet to the interconnection of cells is not treated explicitly in (7). All resistive losses are included in lumped Rs of a solar cell. Parameters of PV module simulations are summarized in Table 1.

The photocurrent I_L, taken to be directly proportional to irradiance (Agbo et al., 2017), is varied between 0.12 and 36 mA/cm^2 which is equivalent to E_e range of approx. 0.003–1 sun. Example set of IV-curves simulated for different irradiances is presented in Fig. 4(a).

3.3. Battery model

The right part of expression (4) - IV characteristic of a battery can be well approximated using a simple battery model referred to as "internal resistance battery model" (Johnson, 2002), or a "zero-time-constant model" (Saidani et al., 2017) describing battery voltage V_B and current I_B by the following expression:

$$V_B = V_{OCB} - R_{sB} I_B, \quad (8)$$

where V_{OCB} is the open circuit voltage of the battery, R_{sB} is the battery total series resistance. The $R_{sB}I_B$ term in (8) represents the overpotential during charging, and loss of potential during discharging (Scrosati, 2013). For a given state of charge the dependence of V_B on I_B is a straight line with a slope of $-1/R_{sB}$ crossing x-axis at V_{OCB}, as presented in Fig. 4 (a) for three V_{OCB} values. Set of parameters for the battery simulations is presented in Table 2. The values correspond to a lab scale battery reported in (Kin et al., 2019).

4. Simulation results

4.1. Room: Power matching in PV-battery unit for PV-harvester

From the analysis given in section 2 it follows that PV-harvester will provide autonomy for a load with $R_L \approx 1$ MΩ per cm^2 of a PV module at minimal allowed office irradiance of approx. 0.003 sun. This high resistance allows to ignore the influence of the load in analysis of power coupling between PV module and battery in this section.

Power matching in PV-harvester is studied with calculation of coupling factor C as a function of irradiance E_e, and battery open circuit voltage V_{OCB}, for a PV module of 7 cells with 1 sun V_{OC} of 4.9 V. An example set of PV module I-V characteristics (IVs) and battery IVs is presented in Fig. 4(a) (note magnified voltage scale). Intersections of the solar module and the battery IVs give working points for each particular combination of V_{OCB} and E_e. One of the possible working points is indicated by a black dot denoted as "WP" in Fig. 4(a). Ideal matching is achieved when the WP dot coincides with a red dot of MPP. One notable feature of battery IVs in Fig. 4(a) is their slope caused by the battery series resistance R_{sB}, which reduces energy efficiency of a battery (Scrosati, 2013) but, on the other hand, makes battery IVs "follow" MPP trajectory, especially at high irradiance 1/4 sun – 1 sun.

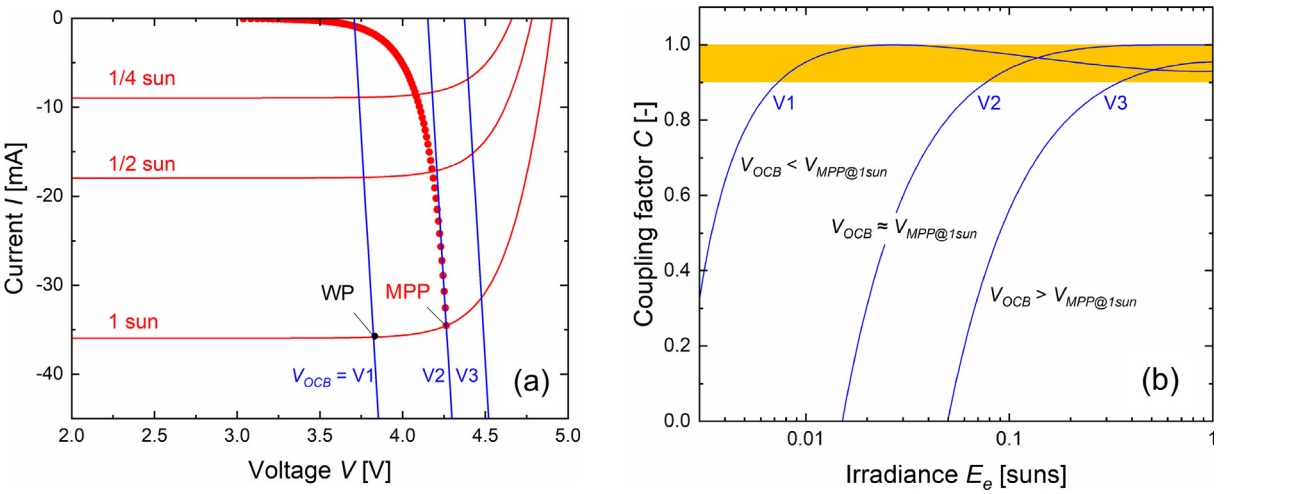

Fig. 4. (a) PV module IVs calculated for different irradiances (red curves), and battery IVs calculated for different V_{OCB}. Red dots show dependence of MPP of the PV module on irradiance. Black dot represents an example of WP at the intersection of the PV module IV and battery IV. Voltage scale is magnified to represent the relevant part of IVs. (b) Dependence of coupling factor C on the irradiance E_e calculated for the PV-battery combinations presented in (a). V1 – combination with $V_{OCB} < V_{MPP@1sun}$, V2 – combination with $V_{OCB} \approx V_{MPP@1sun}$ and V3 – combination with $V_{OCB} > V_{MPP@1sun}$. (For interpretation of the references to colour in this figure legend, the reader is referred to the web version of this article.)

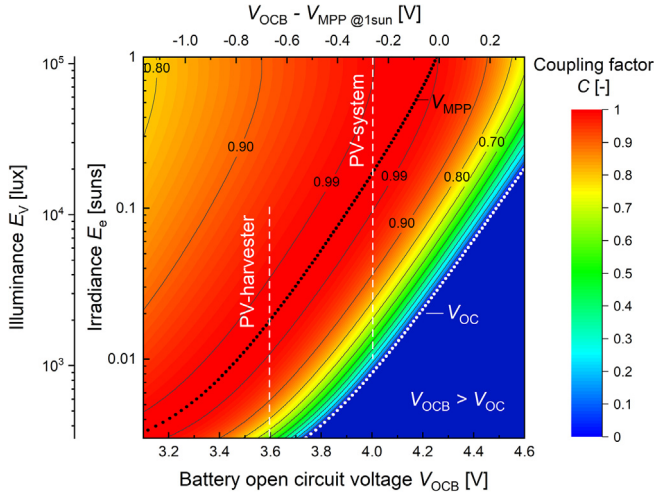

Fig. 5. Contour plot of the dependence of coupling factor C on battery open circuit voltage V_{OCB} and irradiance E_e (illuminance E_V). Scale on top is the difference between V_{OCB} and $V_{MPP@1sun}$. Black dotted line represents dependence of V_{MPP} of solar module on E_e. White dotted line represents dependence of V_{OC} on E_e. For the blue area on the right bottom of V_{OC} line, V_{OCB} exceeds V_{OC} making battery charging impossible. Operating ranges of "PV-harvester" and "PV-system" are indicated with white dashed vertical lines. (For interpretation of the references to colour in this figure legend, the reader is referred to the web version of this article.)

Based on IVs in Fig. 4(a) it is expected that proper combination of PV module and battery will have high coupling factor over wide range of irradiance. This point is illustrated with dependencies of C on irradiance in Fig. 4(b) calculated for three example batteries V1, V2, V3 (V_{OCB} = 3.7 V, 4.15 V, 4.4 V) from Fig. 4(a) representative for three characteristic PV-Battery combinations:

- V1 is a combination with $V_{OCB} < V_{MPP@1sun}$ with high C over wide range of E_e reaching peak value of $C = 1$. The maximum corresponds to a domain in IV-space where the battery IV crosses the trajectory of MPP as irradiance varies. The maximum will shift towards one sun when V_{OCB} is closer to $V_{MPP@1sun}$ and vice versa. This combination shows C between 0.9 and 1 for nearly the whole range of irradiances targeted for PV-harvester in Fig. 1. At high charging current the battery resistive losses are partially compensated with high C due to the slope of the battery IV. Taking into consideration absence of any matching electronics and related power overhead, this case shows very high performance potential of directly coupled PV-battery devices over wide E_e range required for real world indoor or outdoor applications.
- V2 is a PV-battery combination with $V_{OCB} \approx V_{MPP@1sun}$ with $C = 1$ at one sun which drops with reduction of irradiance first slowly down to $E_e \approx 0.1$ sun but then sharply at lower irradiance reaching zero at $E_e \approx 0.02$ sun – the condition when V_{WP} is reduced down to V_{OCB} and charging stops.
- V3 is a combination with too high V_{OCB} exceeding $V_{MPP@1sun}$, where dependence C (E_e) resembles previous case of $V_{OCB} \approx V_{MPP@1sun}$ but ideal matching is not achieved even at 1 sun.

Comprehensive overview of power coupling in various PV-battery combinations under variable irradiance requires calculation of the coupling factor C as a function of two parameters, battery open circuit voltage and irradiance. The result of this calculation, C (V_{OCB}, E_e), is presented as a contour plot in Fig. 5. Additionally, dependencies of V_{MPP} and V_{OC} of the solar module on E_e are shown in Fig. 5 with black and white dotted lines respectively. The area in warm colors on the left of V_{OC} line corresponds to charging mode. The blue area on the right of V_{OC} line represents no-charging mode, i.e. $V_{OCB} > V_{OC}$. Suitable operating ranges of PV-harvester and PV-system are indicated approximately with white dashed vertical lines. The map in Fig. 5, as well as other simulation results presented in this work, is not universal and naturally depend on solar module and battery parameters. Thus, the voltages indicated in Fig. 5 are specific to the simulated PV module and battery. Considerations on practical applications are given at the end of the next section.

The most important outcome of the simulations is the large region with coupling factor $C > 0.9$ which extends over very wide range of irradiance for variety of PV-battery combinations, i.e. the large region where PV-battery combination stays highly power-matched. As it can be seen in the vicinity of a dashed white line "PV-harvester" it is possible to find a combination of V_{OCB} and V_{MPP} which will provide $C \geq 0.9$ for approximately two orders of magnitude of irradiance, $C \geq 0.97$ for one order of magnitude of irradiance, and maximum with $C = 1$. This evidences the potential of directly coupled PV-battery units to be close to modern MPPT devices (Belhachat and Larbes, 2018) as for tracking efficiencies. Unlike tracking efficiencies, the energy

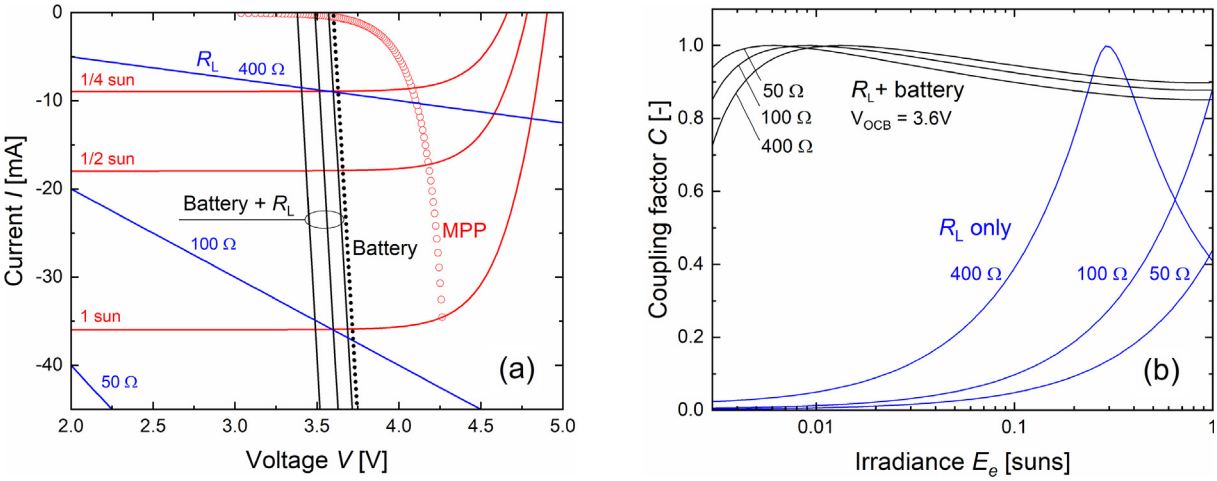

Fig. 6. (a) IVs of a solar module calculated for different irradiances (red curves), IVs of a load resistor calculated for three R_L values 50, 100, and 400 Ω (blue lines), battery IV calculated for V_{OCB} = 3.6 V (dotted black line), common battery-load IVs are presented with black lines, red dots show trajectory of MPP of the solar module with variation of E_e. (b) Dependencies C (E_e) calculated for a combination PV-load without storage (blue lines), and a combination of PV-battery-load (black lines) for elements presented in plot (a). (For interpretation of the references to colour in this figure legend, the reader is referred to the web version of this article.)

Table 1
Parameters for PV module simulation.

Input parameters			Output at 1 sun		
Temperature	T	298.15 K	Open circuit voltage cell	V_{OC}	0.70 V
Saturation current density	J_0	$5.3*10^{-14}$ A/cm^2	MPP current	I_{MPP}	34.5 mA
Ideality factor	n	1	MPP voltage cell	V_{MPP}	0.61 V
Specific series resistance	R_s	0.3 Ω cm^2	Fill factor	FF	83.4%
Specific shunt resistance	R_{sh}	10 kΩ cm^2	Open circuit voltage module	V_{OC}	4.91 V
Short circuit current density at 1 sun	J_{SC}	36 mA/cm^2	MPP voltage module	V_{MPP}	4.27 V
Number of cells	N_C	7	Power at MPP	P_{MPP}	0.147 W
Cell area	A	1 cm^2	Efficiency	η	21%
Irradiance	E_e	0.003–1 sun			

Table 2
Parameters for the battery model.

Parameter		
Open circuit voltage	V_{OCB}	3.1 – 4.6 V
Area specific capacity (1C)		1 mAh/cm^2
Area specific series resistance		75 Ωcm^2
1C area specific current density		1 mA
Area		20 cm^2
Capacity (1C)		20 mAh
Series resistance	R_{sB}	3.75 Ω
1C current	I_{1C}	20 mA

efficiencies are compromised by the power consumption in MPPTs, which plays significant role for PV-harvesters, especially at low irradiance in small scale devices (Giuseppe Marco et al., 2010; Kin et al., 2019). Peak energy efficiency of MPPTs for PV-harvesters ranges between 70% and 90% (Sharma et al., 2018). In contrast, energy efficiency of direct coupling can be very close to the coupling factor, i.e. close to 100% at peak, and therefore has potential to outperform contemporary MPPT devices in small scale low irradiance applications. The direct coupling is expected to be the best option for PV-battery power units for PV-harvesters even for wide irradiance range.

The vertical dashed line "PV-system" shows the case of a system designed for high irradiance and approximately indicates the choice of V_{OCB} with respect to V_{MPP}. The PV-system case is analyzed from R_L point of view in the next section.

The map in Fig. 5 is applicable to analyze matching in PV-battery combinations with realistic dependence of V_{OCB} on SOC (Li et al., 2016; Li et al., 2019). Operating points of a PV-battery combination with variable V_{OCB} will cover an area with width defined by the range of V_{OCB} and height defined by the range of projected irradiance in Fig. 5.

4.2. Roof: Power matching in PV-battery unit with significant load resistance for PV-systems

In contrast to indoor PV-harvesters, PV-systems are designed to operate under high irradiance with coupling to a power demanding load, which results in equivalent specific load resistance R_L of the order of 1 kΩcm^2 as rationalized in section 2. This specific load resistance should be considered in the power matching analysis. Interplay between IV-characteristics of all three elements: PV module, battery, and effective load resistor is analyzed in this section. In Fig. 6(a), PV module IVs for three different irradiances are shown with red lines, IVs of three different load resistances are shown with blue lines, and IV of one battery is shown with black dotted line. Working point of the PV-battery-load combination is located at the intersection of a PV module IV with common battery-load IV according to equation (3). The sums of the battery IV and load IVs are presented with black lines denoted "Battery + R_L" in Fig. 6 (a).

Without a battery the intersection of PV and load IVs will strongly deviate from MPP depending on R_L and irradiance, which is demonstrated by C (E_e) dependencies calculated for three R_L values (blue lines) Fig. 6 (b). It is obvious that for PV module connected to a resistive load, good power matching with $C \geq 0.9$ is achieved for very narrow range of irradiances, thus, utilization of MPPT unit is inevitable to ensure proper matching. However, when battery is connected in parallel to R_L, their common IVs result in completely different matching picture. Slope and x-axis intersection of battery-load IVs (black lines in Fig. 6 (a)) are dominated by the battery IV, and therefore C (E_e)

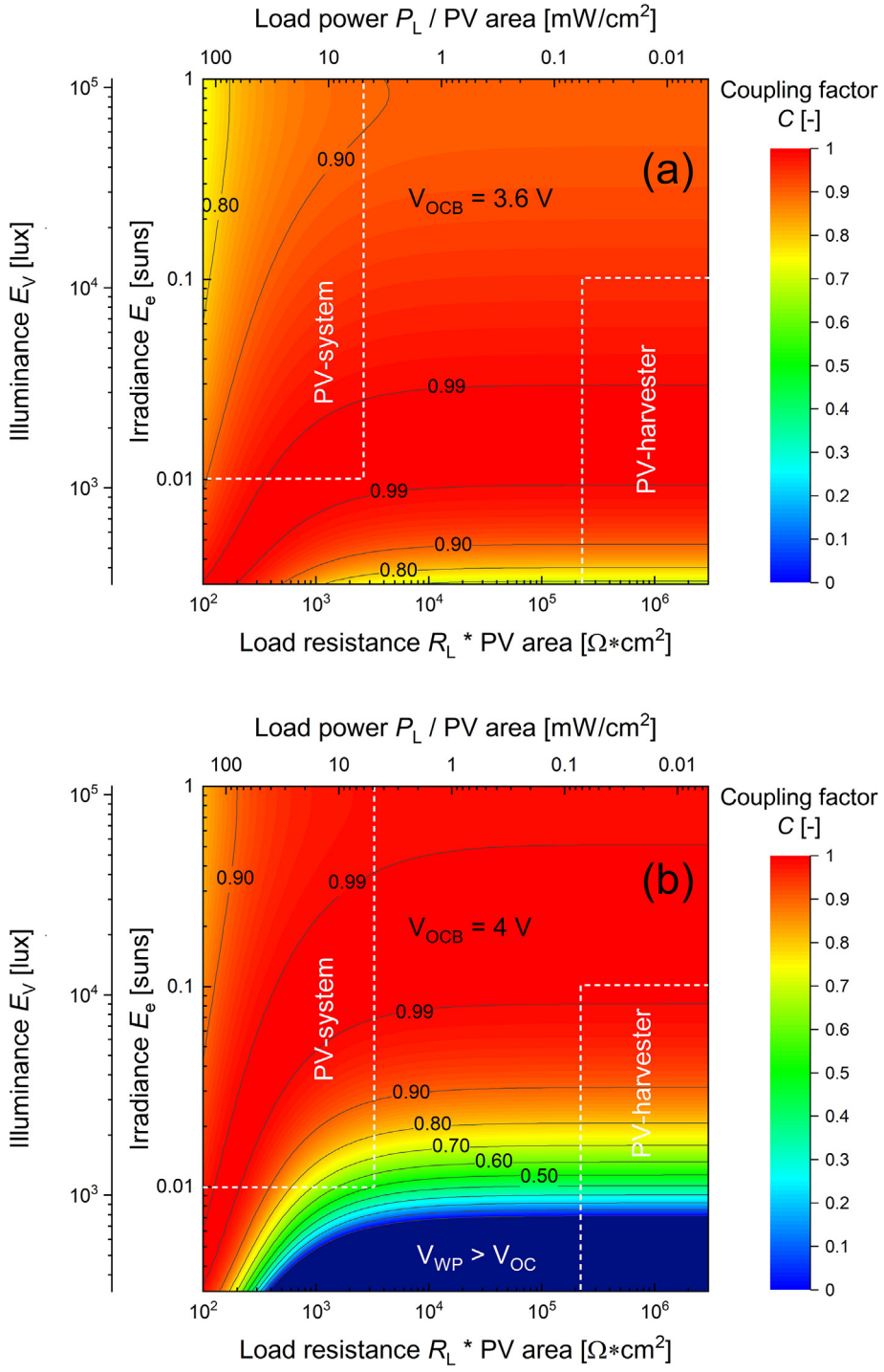

Fig. 7. Coupling factor C as a function of irradiance E_e and specific load resistance R_L calculated for a PV-battery-load combination with two different battery voltages: (a) 3.6 V and (b) 4 V.

dependencies of PV-battery-load combinations show very broad maxima (black "R_L + battery" lines in Fig. 6 (b)). The dependencies of coupling factor on irradiance in PV-batter-load combinations are very similar to the dependencies of the pure PV-battery combinations discussed in previous section (Fig. 4 (b)), i.e. directly coupled PV-battery unit has potential to stay properly matched under wide range of irradiances even under significant load.

A comprehensive overview of power coupling in PV-battery-load is provided via calculation of coupling factor C as a function of load resistance and irradiance. The results are presented as a contour plot of the dependence $C(R_L, E_e)$ in Fig. 7 for two battery voltages: V_{OCB} = 3.6 V in Fig. 7(a) and V_{OCB} = 4 V in Fig. 7(b). These voltages are approximately defined for PV-harvester (3.6 V) and PV-system (4 V) in Fig. 5. The results in Fig. 7(a) simulated for V_{OCB} = 3.6 V show extended domain of $C \geq 0.9$ covering nearly whole studied range with broad maximum at moderate irradiance of 0.005–0.1 sun, and specific $R_L > 1$ kΩ cm^2. These conditions match very well the case of PV-harvester – the area approximately marked on the right side of the graph in Fig. 7(a). Note very wide range of high coupling factor to the left of the marked PV-harvester area. This means that PV-harvester can stay well matched for load resistances much lower than it has been estimated in Fig. 3, which provides stability against fluctuations of R_L

and thereby secures high efficiency of PV-battery unit supplying power to a pulsed load.

Power matching results presented in Fig. 5, for a PV-battery combination without load resistance, indicate that a battery with $V_{OCB} \approx 4$ V is close to be optimally matched to the simulated PV module at high irradiance – the PV-system case. The PV-battery combination with $V_{OCB} = 4$ V is examined now as for the impact of the equivalent specific load resistance. The simulated dependence of coupling factor on R_L, and E_e is presented in Fig. 7(b). The dependence $C(R_L, E_e)$ shows broad maximum with $C > 0.9$ at high E_e and low R_L. The result demonstrates that properly chosen PV-battery combination can preserve excellent power matching from 1 sun down to 0.01 sun independently on load resistance down to specific R_L of 200 Ω*cm^2 (specific power demand of approx. 1000 W/m^2). As well as in the case of PV-harvester, the results in Fig. 7(b) show capability of PV-battery unit to efficiently supply power to appliances operating in DC or pulsed mode without MPPT. In order to compare the potential of direct coupling with MPPT solutions the following has to be taken into consideration. Vast majority of publications are focused on optimization of MPPT algorithms and therefore report "tracking efficiency" or "MPPT efficiency" which can approach 100% very closely (Belhachat and Larbes, 2018; Jiang et al., 2017). The tracking efficiency has to be distinguished from the energy efficiency, which usually has peak values of 93–96% (Abu Qahouq et al., 2014; Cao and Kim, 2015; Cooley and Leeb, 2011). The energy efficiency in MPPT has pronounced dependence on input power which is usually varied within one order of magnitude. As presented in Fig. 7, a directly matched PV-battery unit can have $0.97 > C > 1$ for the irradiance between 0.1 and 1 sun. Taking the absence of power electronics into account these values show potential of the optimized PV-battery unit to be on par with contemporary MPPT solutions as for power efficiency.

Finally, the results presented in Figs. 6 and 7 indicate that battery besides energy storage function may efficiently serve as power matching element in PV-system.

Accurate preselection of PV and battery parameters is fundamental issue of direct coupling, in contrast to MPPT approach. A specific set of experimental parameters is required in order to find proper combination in practice. This set includes several IV characteristics of a PV module measured at different irradiance points of the target irradiance range, and a battery IV characteristic at moderate state of charge. The family of PV module IVs together with the battery IV are used to find working point at each irradiance graphically or numerically as illustrated in Fig. 4(a). Next, coupling factor is determined according to expression (5) and plotted as a function of irradiance as illustrated in Fig. 4(b). The peak of $C(E_e)$ dependence indicates the range of irradiance, where the PV-battery combination performs best. For the case of highly demanding load, common IV of the battery and effective load resistance has to be analyzed as shown in Fig. 6. Practical implementation using standard components may be challenging due to the limited choice of their parameters. Thus, fine tuning of particular PV-battery combinations may require special PV modules, batteries or both.

5. Conclusions

In this work, we explore by means of modeling how far a directly coupled PV-battery unit can stay power-matched under variable irradiance and load. The power coupling in PV-battery unit quantified with coupling factor C has been studied as a function of irradiance E_e, battery voltage V_{OCB} and load resistance R_L. Two distinct utilization cases are analyzed: "PV-harvester" for predominantly low irradiance, non-demanding load, but full system autonomy; and a "PV-system" for predominantly high irradiance, highly demanding load, and partial system autonomy.

It is found that series resistance of a battery may have positive effect on the PV-battery coupling, i.e. the loss related to the battery series resistance can be partially compensated by better matching of PV-battery device.

Dependence of coupling factor C on irradiance E_e and battery voltage V_{OCB} demonstrates that some PV-battery combinations provide $C \geq 0.9$ under irradiance ranging from artificial office lighting to one standard sun, making direct coupling preferable solution for small scale indoor PV-harvesters.

For the case of a PV-system, simulations show that properly chosen PV-battery combination can provide coupling factor of $C \geq 0.9$ for irradiance between 0.03 and 1 sun for specific load resistance ranging from infinity down to 200 Ωcm^2 (equivalent to specific load power demand of 100 mW/cm^2 or 1000 W/m^2), which ensures excellent coupling for most probable application conditions.

We confirm feasibility of intrinsically matched PV-battery combination to provide high power coupling under variety of conditions without MPPT electronics. This result emphasizes the role of a battery as an efficient impedance matching element besides storage functionality in a directly matched PV-system.

Declaration of Competing Interest

The authors declare that they have no known competing financial interests or personal relationships that could have appeared to influence the work reported in this paper.

Acknowledgment

The authors would like to thank Daniel Weigand for fruitful discussion.

References

Abu Qahouq, J.A., Jiang, Y., Orabi, M., 2014. MPPT Control and Architecture for PV Solar Panel with Sub-Module Integrated Converters. Journal of Power Electronics 14(6), 1281–1292.
Agbo, S.N., Merdzhanova, T., Rau, U., Astakhov, O., 2017. Illumination intensity and spectrum-dependent performance of thin-film silicon single and multijunction solar cells. Sol Energ Mat Sol C 159, 427–434.
Agbo, S.N., Merdzhanova, T., Yu, S., Tempel, H., Kungl, H., Eichel, R.-A., Rau, U., Astakhov, O., 2016. Photoelectrochemical application of thin-film silicon triple-junction solar cell in batteries. physica status solidi (a) 213(7), 1926–1931.
Agbo, S.N., Merdzhanova, T., Yu, S.C., Tempel, H., Kungl, H., Eichel, R.A., Rau, U., Astakhov, O., 2016. Development towards cell-to-cell monolithic integration of a thin-film solar cell and lithium-ion accumulator. J Power Sources 327, 340–344.
Alippi, Cesare, Camplani, Romolo, Galperti, Cristian, Roveri, Manuel, 2011. A robust, adaptive, solar-powered WSN framework for aquatic environmental monitoring. IEEE Sens. J. 11 (1), 45–55.
Appelbaum, J., 1989. The operation of loads powered by separate sources or by a common source of solar cells. IEEE Trans. Energy Convers. 4(3), 351–357.
Applebaum, J., 1987. The quality of load matching in a direct-coupling photovoltaic system. IEEE Trans. Energy Convers. EC-2 (4), 534–541.
Averbukh, M., Lineykin, S., Kuperman, A., 2012. Maximum power point matching of solar arrays to arbitrary loads, 2012 IEEE 27th Convention of Electrical and Electronics Engineers in Israel. pp. 1–5.
Awasthi, O.N., 2014. 2014. Alpha Science Internation Limited, Fundamentals of Lighting. New Delhi.
Azzolini, J.A., Tao, M., 2018. A control strategy for improved efficiency in direct-coupled photovoltaic systems through load management. Appl. Energy 231, 926–936.
Bahrami-Yekta, V., Tiedje, T., 2018. Limiting efficiency of indoor silicon photovoltaic devices. Opt. Express 26 (22), 28238. https://doi.org/10.1364/OE.26.028238.
Belhachat, F., Larbes, C., 2018. A review of global maximum power point tracking techniques of photovoltaic system under partial shading conditions. Renew. Sustain. Energy Rev. 92, 513–553.
Belu, R., 2012. Design and analysis of a micro-solar power for Wireless Sensor Networks. In: 2012 9th International Conference on Communications (COMM). pp. 275–278.
Bogue, R., 2012. Solar-powered sensors: a review of products and applications. Sens. Rev. 32 (2), 95–100.
Bunea, G.E., Wilson, K.E., Meydbray, Y., Campbell, M.P., Ceuster, D.M.D., 2006. Low Light Performance of Mono-Crystalline Silicon Solar Cells. In: 2006 IEEE 4th World Conference on Photovoltaic Energy Conference. pp. 1312–1314.
Cao, G., Kim, H.-J., 2015. A novel analog maximum power point tracker for low-cost and low-power distributed PV systems. IEEJ Trans. Electr. Electron. Eng. 10(4), 474–478.
Chen, C., Shang, F., Salameh, M., Krishnamurthy, M., 2018. Challenges and Advancements in Fast Charging Solutions for EVs: A Technological Review. In: 2018 IEEE Transportation Electrification Conference and Expo (ITEC). pp. 695–701.

Chung, W.-Y., Luo, R.-H., Chen, C.-L., Heythem, S., Chang, C.-F., Po, C.-C., 2019. Solar Powered Monitoring System Development for Smart Farming and Internet of Thing Applications. Meeting Abstracts MA2019-01(28), 1371–1371.
Clarke, R.E., Giddey, S., Ciacchi, F.T., Badwal, S.P.S., Paul, B., Andrews, J., 2009. Direct coupling of an electrolyser to a solar PV system for generating hydrogen. Int. J. Hydrogen Energy 34 (6), 2531–2542.
Cooley, J.J., Leeb, S.B., 2011. Per panel photovoltaic energy extraction with multilevel output DC-DC switched capacitor converters, 2011 Twenty-Sixth Annual IEEE Applied Power Electronics Conference and Exposition (APEC). pp. 419–428.
Dehbonei, H., Lee, S.R., Nehrir, H., 2009. Direct energy transfer for high efficiency photovoltaic energy systems Part i: concepts and hypothesis. IEEE Trans. Aerosp. Electron. Syst. 45 (1), 31–45.
Dennler, G., Bereznev, S., Fichou, D., Holl, K., Ilic, D., Koeppe, R., Krebs, M., Labouret, A., Lungenschmied, C., Marchenko, A., Meissner, D., Mellikov, E., Méot, J., Meyer, A., Meyer, T., Neugebauer, H., Öpik, A., Sariciftci, N.S., Taillemite, S., Wöhrle, T., 2007. A self-rechargeable and flexible polymer solar battery. Sol. Energy 81 (8), 947–957.
Dupré, O., Vaillon, R., Green, M.A., 2017. Thermal Behavior of Photovoltaic Devices.
El Fadil, H., Giri, F., 2011. Climatic sensorless maximum power point tracking in PV generation systems. Control Eng. Pract. 19 (5), 513–521.
Gibson, T, Kelly, N, 2008. Optimization of solar powered hydrogen production using photovoltaic electrolysis devices. Int. J. Hydrogen Energy 33 (21), 5931–5940.
Giuseppe Marco, T., Cristina, V., Paolo, A., Luca, P., Dario, G.A., Massimo, P., 2010. Design considerations about a photovoltaic power system to supply a mobile robot, 2010 IEEE International Symposium on Industrial Electronics. pp. 1829–1834.
Guo, W., Xue, X., Wang, S., Lin, C., Wang, Z.L., 2012. An integrated power pack of dye-sensitized solar cell and Li battery based on double-sided TiO2 nanotube arrays. Nano Lett 12(5), 2520–2523.
Gurung, A., Chen, K., Khan, R., Abdulkarim, S.S., Varnekar, G., Pathak, R., Naderi, R., Qiao, Q., 2017. Highly efficient perovskite solar cell photocharging of lithium ion battery using DC-DC booster. Adv. Energy Mater. 7 (11), 1602105.
Gurung, A., Qiao, Q., 2018. Solar charging batteries: advances, challenges, and opportunities. Joule 2 (7), 1217–1230.
Hauch, A., Georg, A., Krašovec, U. Opara, Orel, B., 2002. Photovoltaically self-charging battery. J. Electrochem. Soc. 149 (9), A1208.
Hosono, E., Matsuda, H., Honma, I., Ichihara, M., Zhou, H., 2007. High-Rate Lithium Ion Batteries with Flat Plateau Based on Self-Nanoporous Structure of Tin Electrode. Journal of The Electrochemical Society 154(2).
Hu, Y., Bai, Y., Luo, B., Wang, S., Hu, H., Chen, P., Lyu, M., Shapter, Joe, Rowan, A., Wang, L., 2019. A portable and efficient solar-rechargeable battery with ultrafast photo-charge/discharge rate. Adv. Energy Mater. 9 (28), 1900872.
Hua, C., Lin, J., Tzou, H., 2003. MPP control of a photovoltaic energy system. Euro. Trans. Electr. Power 13 (4), 239–246.
International, A., 2012. ASTM G173-03(2012), Standard Tables for Reference Solar Spectral Irradiances: Direct Normal and Hemispherical on 37° Tilted Surface. West Conshohocken, PA, USA.
Jaboori, M.G., Saied, M.M., Hanafy, A.A.R., 1991. A contribution to the simulation and design optimization of photovoltaic systems. IEEE Trans. Energy Convers. 6(3), 401–406.
Jiang, J.-A., Su, Y.-L., Kuo, K.-C., Wang, C.-H., Liao, M.-S., Wang, J.-C., Huang, C.-K., Chou, C.-Y., Lee, C.-H., Shieh, J.-C., 2017. On a hybrid MPPT control scheme to improve energy harvesting performance of traditional two-stage inverters used in photovoltaic systems. Renewable and Sustainable Energy Reviews 69, 1113–1128.
Johnson, V.H., 2002. Battery performance models in ADVISOR. J. Power Sources 110 (2), 321–329.
Julien, C.M., Mauger, A., 2013. Review of 5-V electrodes for Li-ion batteries: status and trends. Ionics 19 (7), 951–988.
Kakimoto, N., Asano, R., 2017. Linear operation of photovoltaic array with directly connected lithium-ion batteries. IEEE Trans. Sustain. Energy 8 (4), 1647–1657.
Khouzam, Kamel, Khouzam, Lucy, Groumpos, Peter, 1991. Optimum matching of ohmic loads to the photovoltaic array. Sol. Energy 46 (2), 101–108.
Khouzam, K.Y., 1990. Optimum load matching in direct-coupled photovoltaic power systems-application to resistive loads. IEEE Trans. Energy Convers. 5(2), 265–271.
Khouzam, K.Y., Khouzam, L., 1991. Optimum matching of a photovoltaic array to a storage battery, The Conference Record of the Twenty-Second IEEE Photovoltaic Specialists Conference - 1991. pp. 706–711 vol. 701.
Kin, L.-C., liu, z., Astakhov, O., Agbo, S.N., Tempel, H., Yu, S., Kungl, H., Eichel, R.-A., Rau, U., Kirchartz, T., Merdzhanova, T., 2019. Efficient area matched converter aided solar charging of lithium ion batteries using high voltage perovskite solar cells. ACS Appl. Energy Mater.
Kou, Q., Klein, S.A., Beckman, W.A., 1998. A method for estimating the long-term performance of direct-coupled PV pumping systems. Sol. Energy 64 (1-3), 33–40.
Li, C., Islam, M.M., Moore, J., Sleppy, J., Morrison, C., Konstantinov, K., Dou, S.X., Renduchintala, C., Thomas, J., 2016. Wearable energy-smart ribbons for synchronous energy harvest and storage. Nat Commun 7, 13319.
Li, W., Fu, H.-C., Zhao, Y., He, J.-H., Jin, S., 2018. 14.1% Efficient Monolithically Integrated Solar Flow Battery. Chem 4(11), 2644–2657.
Li, W., Fu, H.C., Li, L., Caban-Acevedo, M., He, J.H., Jin, S., 2016. Integrated Photoelectrochemical Solar Energy Conversion and Organic Redox Flow Battery Devices. Angew Chem Int Ed Engl 55(42), 13104-13108.
Li, W., Kerr, E., Goulet, M.A., Fu, H.C., Zhao, Y., Yang, Y., Veyssal, A., He, J.H., Gordon, R. G., Aziz, M.J., Jin, S., 2019. A Long Lifetime Aqueous Organic Solar Flow Battery. Adv Energy Mater 9(31).
Liu, P., Yang, H.X., Ai, X.P., Li, G.R., Gao, X.P., 2012. A solar rechargeable battery based on polymeric charge storage electrodes. Electrochemistry Communications 16(1), 69–72.
Maeda, T., Ito, H., Hasegawa, Y., Zhou, Z., Ishida, M., 2012. Study on control method of the stand-alone direct-coupling photovoltaic – Water electrolyzer. Int. J. Hydrogen Energy 37 (6), 4819–4828.
Maroufmashat, A., Sayedin, F., Khavas, S.S., 2014. An imperialist competitive algorithm approach for multi-objective optimization of direct coupling photovoltaic-electrolyzer systems. Int. J. Hydrogen Energy 39 (33), 18743–18757.
Masoum, M.A.S., Dehbonei, H., Fuchs, E.F., 2002. Theoretical and experimental analyses of photovoltaic systems with voltageand current-based maximum power-point tracking. IEEE Trans. Energy Convers. 17(4), 514–522.
Merei, G., Moshövel, J., Magnor, D., Sauer, D.U., 2016. Optimization of self-consumption and techno-economic analysis of PV-battery systems in commercial applications. Appl. Energy 168, 171–178.
Merten, J., Asensi, J.M., Voz, C., Shah, A.V., Platz, R., Andreu, J., 1998. Improved equivalent circuit and analytical model for amorphous silicon solar cells and modules. IEEE Trans. Electron Dev. 45(2), 423–429.
Millet, L., Berrueta, A., Bruch, M., Reiners, N., Vetter, M., 2019. Extensive analysis of photovoltaic battery self-consumption: evaluation through an innovative district case-study. Appl. Phys. Rev. 6 (2), 021301. https://doi.org/10.1063/1.5049665.
Mokeddem, A., Midoun, A., Kadri, D., Hiadsi, S., Raja, I.A., 2011. Performance of a directly-coupled PV water pumping system. Energy Convers. Manage. 52 (10), 3089–3095.
Paul Ayeng'o, S., Axelsen, H., Haberschusz, D., Sauer, D.U., 2019. A model for direct-coupled PV systems with batteries depending on solar radiation, temperature and number of serial connected PV cells. Sol. Energy 183, 120–131.
Roscher, M.A., Bohlen, O., Vetter, J., 2011. OCV hysteresis in Li-Ion batteries including two-phase transition materials. Int. J. Electrochem. 2011, 1–6.
Saidani, F., Hutter, F.X., Scurtu, R.-G., Braunwarth, W., Burghartz, J.N., 2017. Lithium-ion battery models: a comparative study and a model-based powerline communication. Advances in Radio Science 15, 83-91.
Sandbaumhuter, F., Agbo, S.N., Tsai, C.L., Astakhov, O., Uhlenbruck, S., Rau, U., Merdzhanova, T., 2017. Compatibility study towards monolithic self-charging power unit based on all-solid thin-film solar module and battery. J Power Sources 365, 303–307.
Scrosati, B., 2013. Lithium batteries: advanced technologies and applications [E-Book]. John Wiley & Sons, Inc., Hoboken, NJ.
Shao, H., Tsui, C.-Y., Ki, W.-H., 2009. The design of a micro power management system for applications using photovoltaic cells with the maximum output power control. IEEE Trans. VLSI Syst. 17 (8), 1138–1142.
Sharma, H., Haque, A., Jaffery, Z.A., 2018. Solar energy harvesting wireless sensor network nodes: a survey. J. Renew. Sustain. Energy 10 (2).
Smirnov, V., Welter, K., Becker, J.-P., Urbain, F., Jaegermann, W., Finger, F., 2016. The effect of the illumination intensity on the performance of Si multijunction based integrated photoelectrochemical water splitting devices. Energy Procedia 102, 36–42.
Standartization, E.C.f., 2002. Light and lighting - Lighting of work places, Part 1: Indoor work places.
Standartization, E.C.f., 2014. Light and lighting - Lighting of work places, Part 2: Outdoor work places.
Su, Z., Ding, S., Gan, Z., Yang, X., 2016. Analysis of a photovoltaic-electrolyser direct-coupling system with a V-trough concentrator. Energy Convers. Manage. 108, 400–410.
Sun, X., Radovanovic, P.V., Cui, B., 2015. Advances in spinel Li 4 Ti 5 O 12 anode materials for lithium-ion batteries. New J. Chem. 39 (1), 38–63.
Tiwari, A.K., Kalamkar, V.R., 2016. Performance investigations of solar water pumping system using helical pump under the outdoor condition of Nagpur, India. Renew. Energy 97, 737–745.
Urbain, F., Smirnov, V., Becker, J.-P., Lambertz, A., Yang, F., Ziegler, J., Kaiser, B., Jaegermann, W., Rau, U., Finger, F., 2016. Multijunction Si photocathodes with tunable photovoltages from 2.0 V to 2.8 V for light induced water splitting. Energy Environ. Sci. 9 (1), 145–154.
Urbain, F., Wilken, K., Smirnov, V., Astakhov, O., Lambertz, A., Becker, J.-P., Rau, U., Ziegler, J., Kaiser, B., Jaegermann, W., Finger, F., 2014. Development of thin film amorphous silicon tandem junction based photocathodes providing high open-circuit voltages for hydrogen production. Int. J. Photoenergy 2014, 1–10.
Vega-Garita, V., Ramirez-Elizondo, L., Narayan, N., Bauer, P., 2019. Integrating a photovoltaic storage system in one device: a critical review. Prog. Photovolt. Res. Appl. 27 (4), 346–370.
Wang, Y., Ji, J., Sun, W., Yuan, W., Cai, J., Guo, C., He, Wei, 2016. Experiment and simulation study on the optimization of the PV direct-coupled solar water heating system. Energy 100, 154–166.
Weniger, J., Tjaden, T., Quaschning, V., 2014. Sizing of residential PV battery systems. Energy Procedia 46, 78–87.
Zaghib, K., Dontigny, M., Guerfi, A., Charest, P., Rodrigues, I., Mauger, A., Julien, C.M., 2011. Safe and fast-charging Li-ion battery with long shelf life for power applications. J. Power Sources 196 (8), 3949–3954.
Zeng, Q., Lai, Y., Jiang, L., Liu, F., Hao, X., Wang, L., Green, M.A., 2020. Integrated photorechargeable energy storage system: next-generation power source driving the future. Adv. Energy Mater. 10 (14).
Zhang, R., Xia, B., Li, B., Cao, L., Lai, Y., Zheng, W., Wang, H., Wang, W., 2018. State of the art of lithium-ion battery SOC estimation for electrical vehicles. Energies 11(7).